15th World Congress on Computational Mechanics (WCCM-XV)
8th Asian Pacific Congress on Computational Mechanics (APCOM-VIII)
Virtual Congress: 31 July – 5 August 2022
S. Koshizuka (Ed.)

TEXTURE SHAPE OPTIMIZATION FOR MINIMIZATION OF FRICTION COEFFICIENT (COMPARISON OF SHAPE OPTIMIZATION RESULTS FOR CIRCULAR AND HERRINGBONE TEXTURE)

H. ARATA[1], T. KURAHASHI[2]

[1]Nagaoka University of Technology
1603-1, Kamitomiokamachi
Nagaoka, Niigata, Japan
Email address; s193009@stn.nagaokaut.ac.jp

[2]Nagaoka University of Technology
1603-1, kamitomiokamati
Nagaoka, Niigata, Japan
Email address; kurahashi@mech.nagaokaut.ac.jp

Key words: Shape Optimization, Adjoint Variable Method, Finite Element Method, Friction Coefficient, Circular Texture, Herringbone Texture.

Abstract. *In order to reduce the friction coefficient of lubricated surfaces with circular and herringbone shaped textures, an adjust variable method was introduced to optimize the shape of the oil film thickness distribution in the textured areas. The optimized oil film thickness distribution can be evolved by the shape updating formula proposed by Sasaoka et al. based on the smoothed sensitivity. For computational convenience, the objective function in the optimization is defined as the friction force, not the friction coefficient. The constraint function was also defined by the Reynolds equation. The finite element method was used in the optimization procedure. The optimization results show that the herringbone shape texture has a bowl-shaped oil film thickness distribution similar to that of the circular shape texture. Furthermore, the location of the deepest part was found to be different.*

1 INTRODUCTION

In recent years, as environmental problems caused by global warming have become more apparent, there has been a growing movement toward the realization of a sustainable society. In order to realize a sustainable society, it is essential to reduce energy consumption through lower friction. One method to reduce friction is a surface modification technique called surface texturing. This involves the processing of microscopic bumps and grooves on sliding surfaces. This type of processing technology has been used for a relatively long time, and "kisage processing" is a typical example. In recent years, with the development of microfabrication technology, the scope of application has expanded to sliding surfaces such as bearings and piston rings. In general, it is known that the lubricating performance of sliding surfaces is highly dependent on the shape of the texture. The optimal texture shape also depends on the lubrication

condition of sliding surfaces and sliding conditions. Therefore, numerous studies have been conducted to obtain the optimum parameters and texture shape. The first research on surface texturing was conducted by D.B. Hamilton et al. in 1966, which showed that minute irregularities add hydrodynamic value and affect pressure and load capacity [1]. Then in 1996, I. Etsion et al. presented a model of a mechanical seal with a microscopic surface structure and showed that a uniform distribution of hemispherical dimples can significantly improve the sealing performance [2]. In 2007, H.L. Costa et al. performed detailed experiments on circles, grooves, and chevrons and showed that chevrons increase fluid film thickness more than circles and grooves [3]. In 2015, C. Shen et al. performed numerical optimization based on the SQP algorithm to maximize the LCC of textures and proposed a chevron shape for unidirectional slides and a trapezoidal shape for bidirectional slides [4]. In 2020, S. Sasaoka et al. performed shape optimization of the oil film thickness distribution to minimize the friction coefficient for circular textures and obtained a parabolic shape [5]. In 2021, H. Kodama et al. performed CFD analysis for herringbone grooves with constant depth and herringbone grooves with sloping depth. The results showed that the herringbone groove with sloping depth increased the dynamic pressure at the groove tip and decreased the circumferential dynamic pressure variation [6]. In 2021, Z. Shan et al. found that the chevron configuration affects the pressure distribution, which in turn affects the load capacity and friction coefficient. They also proposed a V-shaped arrangement and showed that it improves lubrication performance [7]. In 2021, T. Zhirong performed shape optimization using the level set method to maximize LCC and obtained a chevron shape [8]. From these results, it can be said that the herringbone (chevron) pattern can increase the load capacity and improve lubrication performance. In addition, there is no geometry optimization of herringbone groove depth to maximize load capacity or minimize the coefficient of friction. Therefore, the objective of this study was to optimize the shape of the herringbone texture depth to minimize the friction coefficient. We also compare our results with those presented by S. Sasaoka et al.

2 FORMULATION OF THE SHAPE OPTIMIZATION PROBLEM

2.1 CALCULATION MODEL

As shown in Fig.1, the domain Ω is a textured surface. It consists of a untextured domain Ω_1 and textured domain Ω_2 separated by an interface Γ_2. The boundary of Ω is defined as

$$\Omega = \Gamma_1 \cup \Gamma_2 \tag{1}$$

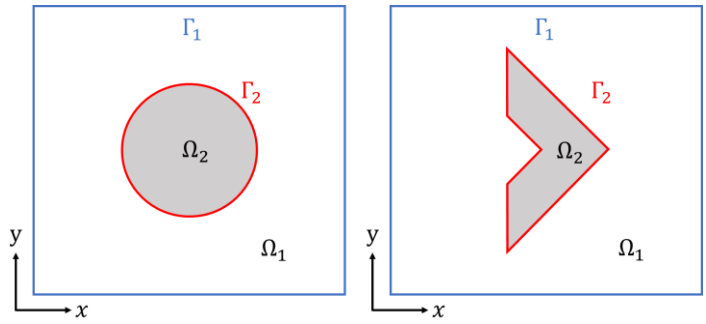

Fig.1 Computational domain

The Reynolds equation shown as Eq. (2) and is a simplified lubrication equation.

$$\frac{\partial}{\partial \mathrm{x}}\left(ph^3\frac{\partial p}{\partial x}\right)+\frac{\partial}{\partial \mathrm{y}}\left(ph^3\frac{\partial p}{\partial y}\right)=6\eta U\frac{\partial}{\partial x}(ph) \tag{2}$$

With the boundary condition,

$$\mathrm{p}=0 \text{ on } \Gamma_1 \text{ and } \mathrm{p} < 0 \tag{3}$$

where x and y are the Cartesian coordinates, p is the film pressure, h is the film thickness, η is the viscosity, U is the sliding velocity. h is given by

$$h=\begin{cases} h_0 & in\ \Omega_1 \\ h_0+h_v & in\ \Omega_2 \end{cases} \tag{4}$$

here h_v is the depth of textures.

In lubricated contacts with surface textures, it is important to reduce the coefficient of friction. In this study, the friction force of the molecule of friction coefficient was selected as the optimization target. The objective function F is expressed as,

$$F=\int_\Omega\left(\frac{\eta U}{h}+\frac{h}{2}\frac{dp}{dx}\right)d\Omega \tag{5}$$

The optimization problem can be expressed in the following equation,

$$\min: J=F \tag{6}$$

From the next section, the Reynolds equation is expressed as,

$$\frac{\partial^2 p}{\partial x^2}+\frac{\partial^2 p}{\partial y^2}+\frac{3}{h}\left(\frac{\partial h}{\partial x}\frac{\partial p}{\partial x}+\frac{\partial h}{\partial y}\frac{\partial p}{\partial x}\right)=\frac{6\eta U}{h^3}\frac{\partial h}{\partial x} \tag{7}$$

2.2 OPTIMIZATION PROBLEMS

The optimization problem can be defined as a minimization problem of Lagrange function, which is expressed as,

$$L = \int_\Omega \left(\frac{\eta U}{h} + \frac{h}{2}\frac{dp}{dx}\right) \mathrm{d}\Omega + \int_\Omega \left[\frac{\partial^2 p}{\partial x^2} + \frac{\partial^2 p}{\partial y^2} + \frac{3}{h}\left(\frac{\partial h}{\partial x}\frac{\partial p}{\partial x} + \frac{\partial h}{\partial y}\frac{\partial p}{\partial x}\right) - \frac{6\eta U}{h^3}\frac{\partial h}{\partial x}\right] \lambda \, \mathrm{d}\Omega \tag{8}$$

where q is the adjoint pressure. where the partial derivative of L with respect to λ is the equation of state. Then, the first variant of the Lagrange function is obtained based on the variational principle, which leads to the following equation.

$$\begin{aligned}
\delta L = & \int_\Omega \ \delta\lambda \left[\frac{\partial^2 p}{\partial x^2} + \frac{\partial^2 p}{\partial y^2} + \frac{3}{h}\left(\frac{\partial p}{\partial x}\frac{\partial h}{\partial x} + \frac{\partial p}{\partial y}\frac{\partial h}{\partial y}\right) - \frac{6\eta U}{h^3}\frac{\partial h}{\partial x}\right] \mathrm{d}\Omega \\
& + \int_\Omega \ \delta p \left[-\frac{1}{2}\frac{\partial h}{\partial x} + \frac{\partial^2 \lambda}{\partial x^2} + \frac{\partial^2 \lambda}{\partial y^2} - \frac{3}{h}\left(\frac{\partial \lambda}{\partial x}\frac{\partial h}{\partial x} + \frac{\partial \lambda}{\partial y}\frac{\partial h}{\partial y}\right) + \frac{3\lambda}{h^2}\left(\frac{\partial h}{\partial x}\frac{\partial h}{\partial x} + \frac{\partial h}{\partial y}\frac{\partial h}{\partial y}\right) - \frac{3\lambda}{h}\left(\frac{\partial^2 h}{\partial x^2} + \frac{\partial^2 h}{\partial y}\right)\right] \mathrm{d}\Omega \\
& + \int_\Omega \ \delta h \left[-\frac{\eta U}{h^2} + \frac{1}{2}\frac{\partial p}{\partial x} - \frac{3}{h}\left(\frac{\partial \lambda}{\partial x}\frac{\partial p}{\partial x} + \frac{\partial \lambda}{\partial y}\frac{\partial p}{\partial y}\right) - \frac{3\lambda}{h}\left(\frac{\partial^2 p}{\partial x^2} + \frac{\partial^2 p}{\partial y}\right) + \frac{6\eta U}{h^3}\frac{\partial \lambda}{\partial x}\right] \mathrm{d}\Omega \\
& + \int_{\Gamma_1} \left[\delta p \left(\frac{3\lambda}{h}\frac{\partial h}{\partial y} - \frac{\partial \lambda}{\partial y}\right) + \delta \frac{\partial p}{\partial y}(\lambda) + \delta h \left(\frac{3\lambda}{h}\frac{\partial p}{\partial y}\right)\right] n_x \mathrm{d}\Omega \\
& + \int_{\Gamma_1} \left[\delta p \left(\frac{h}{2} + \frac{3\lambda}{h}\frac{\partial h}{\partial x} - \frac{\partial \lambda}{\partial y}\right) + \delta \frac{\partial p}{\partial x}(\lambda) + \delta h \left(\frac{3\lambda}{h}\frac{\partial p}{\partial y} - \frac{6\eta U}{h^3}\right)\right] n_y \mathrm{d}\Omega = 0
\end{aligned} \tag{9}$$

Consequently, Eq. (10) is derived. It is the adjoint equation.

$$\int_\Omega \left[-\frac{1}{2}\frac{\partial h}{\partial x} + \frac{\partial^2 \lambda}{\partial x^2} + \frac{\partial^2 \lambda}{\partial y^2} - \frac{3}{h}\left(\frac{\partial \lambda}{\partial x}\frac{\partial h}{\partial x} + \frac{\partial \lambda}{\partial y}\frac{\partial h}{\partial y}\right) + \frac{3\lambda}{h^2}\left(\frac{\partial h}{\partial x}\frac{\partial h}{\partial x} + \frac{\partial h}{\partial y}\frac{\partial h}{\partial y}\right) - \frac{3\lambda}{h}\left(\frac{\partial^2 h}{\partial x^2} + \frac{\partial^2 h}{\partial y}\right)\right] \mathrm{d}\Omega = 0 \tag{10}$$

Similarly, the gradient of the Lagrange function with respect to oil film thickness is also derived.

$$\frac{\partial \mathrm{L}}{\partial \mathrm{h}} = -\frac{\eta U}{h^2} + \frac{1}{2}\frac{\partial p}{\partial x} - \frac{3}{h}\left(\frac{\partial \lambda}{\partial x}\frac{\partial p}{\partial x} + \frac{\partial \lambda}{\partial y}\frac{\partial p}{\partial y}\right) - \frac{3\lambda}{h}\left(\frac{\partial^2 p}{\partial x^2} + \frac{\partial^2 p}{\partial y}\right) + \frac{6\eta U}{h^3}\frac{\partial \lambda}{\partial x} \tag{11}$$

2.3 WEAK FORMS

The weak forms of Eq. (7) are shown in Eq. (12).

$$\int_\Omega \left[-h^3\left(\frac{\partial p^*}{\partial x}\frac{\partial p}{\partial x} + \frac{\partial p^*}{\partial y}\frac{\partial p}{\partial y}\right) + 3h^2 p^*\left(\frac{\partial p}{\partial x}\frac{\partial h}{\partial x} + \frac{\partial p}{\partial y}\frac{\partial h}{\partial y}\right)\right] d\Omega - \int_\Omega \left[6\eta U p^* \frac{\partial h}{\partial x}\right] d\Omega$$

$$+\int_{\Gamma_1}\left[p^* h^3\left(\frac{\partial p}{\partial x}n_x+\frac{\partial p}{\partial y}n_y\right)\right]d\Gamma_1=0 \tag{12}$$

Similarly, the weak forms of Eq. (10) are shown in Eq. (13).

$$\int_\Omega\left[-\left(\frac{\partial\lambda^*}{\partial x}h^3+3\lambda^* h^2\frac{\partial h}{\partial x}\right)\frac{\partial\lambda}{\partial x}-\left(\frac{\partial\lambda^*}{\partial y}h^3+3\lambda^* h^3\frac{\partial h}{\partial y}\right)\frac{\partial\lambda}{\partial y}+3\lambda^* h^2\left(\frac{\partial\lambda}{\partial x}+\frac{\partial\lambda}{\partial y}\right)\right]d\Omega$$

$$-\int_\Omega\left[\left(\lambda^*\frac{h}{2}-\frac{\partial\lambda^*}{\partial x}\frac{h^2}{4}+\lambda^*\frac{h}{2}\frac{\partial h}{\partial x}\right)\frac{\partial p}{\partial x}\right]d\Omega-\int_{\Gamma_1}\left[\lambda^* h^3\frac{\partial\lambda}{\partial x}n_x+\lambda h^3\frac{\partial\lambda}{\partial y}n_y\right]d\Gamma_1$$

$$-\int_{\Gamma_1}\left[\lambda^*\frac{h^2}{4}\frac{\partial p}{\partial x}n_x\right]d\Gamma_1=0 \tag{13}$$

3 CALCULATION PROCEDURE

The calculation procedure is as follows.

1. Input of computational conditions and setting a computational model.

2. Pressure field analysis of the governing equation.

3. When the pressure is integrated and the load obtained is close to the set value, proceed to the next step. If not, update the basic oil film thickness and return to 2.

4. Compute the performance function and the convergence detection formula$|(J^{n+1}-J^n/J^0)|$ and end the computation if it is smaller than the convergence criterion ϵ. If not, proceed to the next step.

5. Compute adjoint variables based on the adjoint equations.

6. Compute the gradient of oil film thickness $\partial L/\partial h$.

7. Smooth the gradient by applying Poisson equation.

8. Update the shape by Sasaoka's proposed shape update formula [5] and return to 2.

4 CALCULATION CONDITIONS

The calculation conditions are shown in Table 1.

Table 1: Calculation condition

Shape of texture	circle	herringbone
Number of nodes	20722	20511
Number of elements	41122	40700
Load W [N]	10	10
Sliding speed U [mm/s]	1000	1000
Convergence test constant ε [-]	10^{-4}	10^{-4}
Viscosity coefficient η [Pa・s]	0.08	0.08
Initial depth of texture h_{dep} [mm]	0.01	0.01
Percentage of texture [%]	35.051	34.996

The finite element mesh is shown in Fig.2.

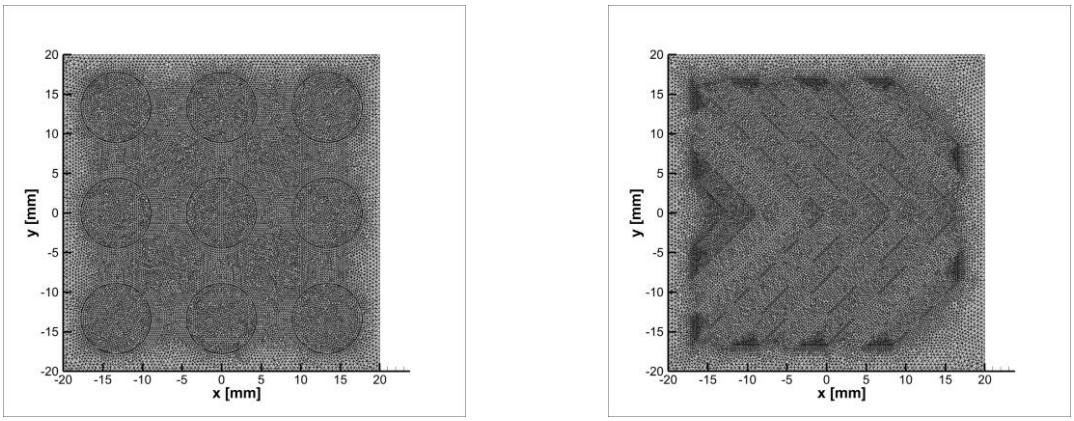

Fig.2 Finite element mesh (Left: Circle, Right: Herringbone)

The initial shape is shown in Fig.3.

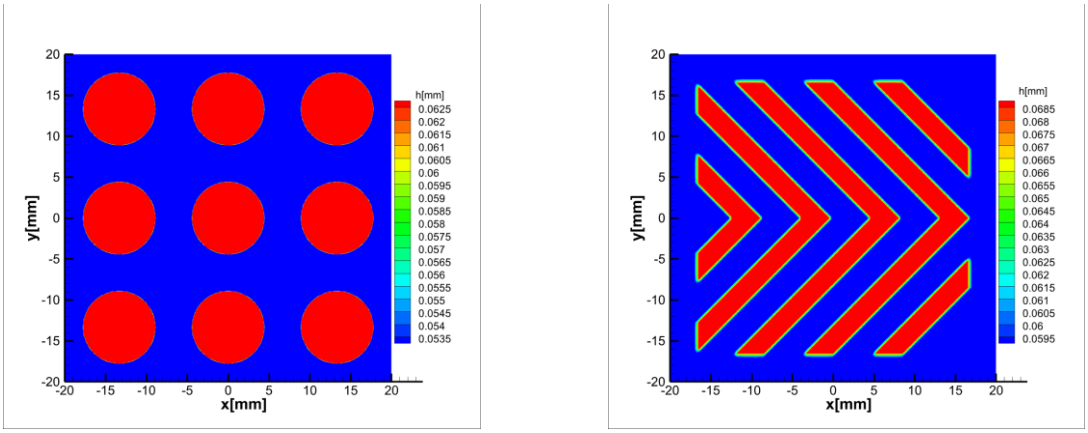

Fig.3 Initial shape (Left: Circle, Right: Herringbone)

5 COMPARISON OF FINAL SHAPE

The history of friction coefficients is shown in Fig.4.

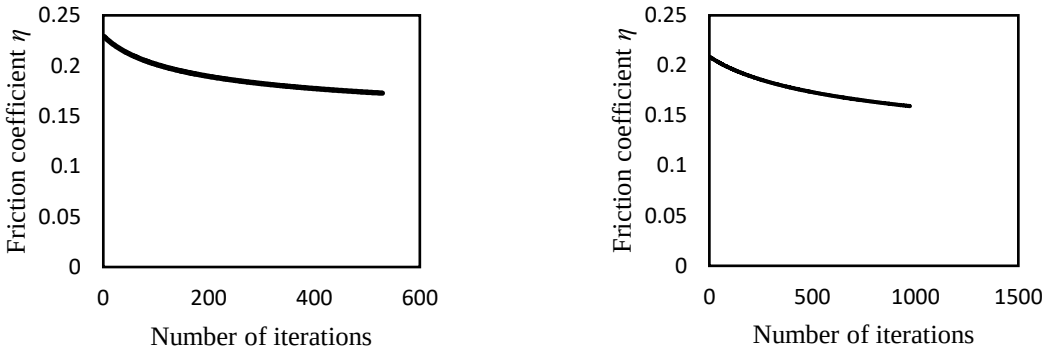

Fig.4 History of friction coefficient (Left: Circle, Right: Herringbone)

The final shape obtained by the calculation is shown in Fig.5.

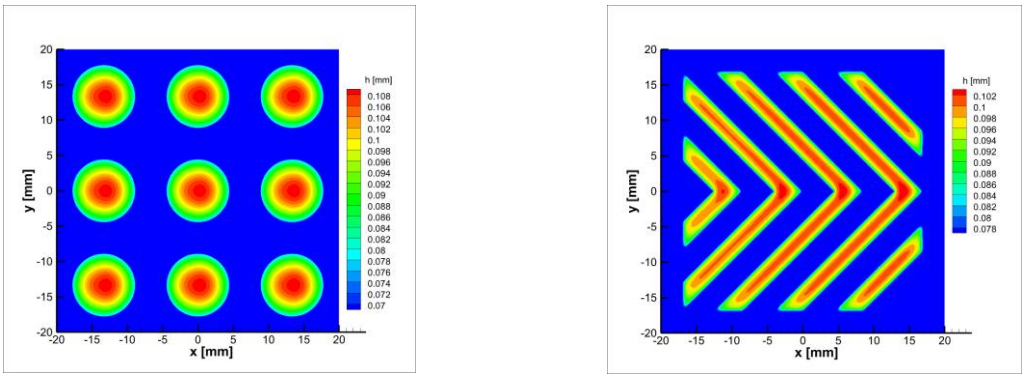

Fig.5 Final shape of oil film thickness distribution (Left: Circle, Right: Herringbone)

The pressure distribution of the final shape is shown in Fig.6.

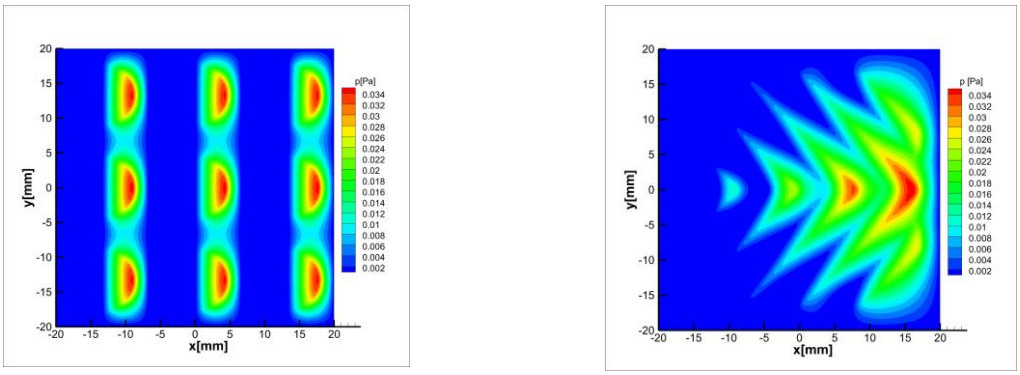

Fig.6 Pressure distribution of the final shape (Left: Circle, Right: Herringbone)

As can be seen the Fig.4, friction coefficient is significantly reduced by shape optimization. In particular, it can be seen that friction coefficient of the herringbone texture when the calculation is end, lower than friction coefficient of circular texture. Also, as can be seen the Fig.5, the circular texture has the deepest point at the center of the circle. On the other hand, the herringbone texture has the deepest point near the apex of the herringbone. And, then, If the herringbone texture of results in Fig.5 and Fig.6 are compared, it can be seen that the depth increases at the pressure high area.

6 ASSESSMENT OF SPEED EFFECT

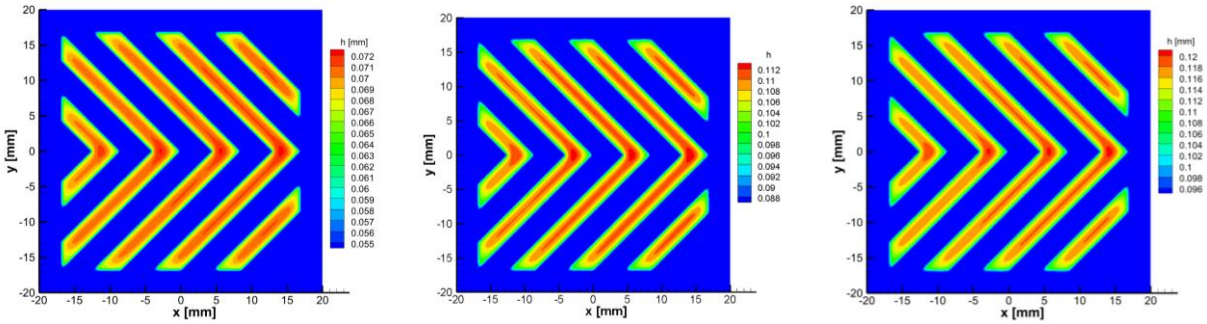

500 m/s 1000 m/s 2000 m/s

Fig.7 Comparison of different speeds

As can be seen the Fig.7, the shape optimization of the herringbone texture was performed at different sliding speeds. It The previously mentioned characteristics are more pronounced at high speeds.

7 CONCLUSIONS

In this study, the shape optimization of oil film thickness of herringbone texture was performed to minimize the friction coefficient by the adjoint variable method. As a result, the following conclusions were obtained.

- The results show that the optimal depth shape of the herringbone texture has characteristic protrusions that lower the friction coefficient.
- The reason for the appearing the characteristic protrusions may be due to the increased pressure at the top of the herringbone.
- The characteristic protrusions become more pronounced as the speed increases.
- Herringbone textures have a lower friction coefficient than circular textures.

From these results, it can be concluded that it is possible to obtain herringbone textured groove shapes with a lower friction coefficient than previously possible. However, the groove shape has also been examined from other perspectives. For example, Kodama et al. have proposed herringbone texture grooves that enhance hydrodynamic effects [6]. Specifically, the groove depth is made shallower toward the sliding direction. From these, it can be seen that the results are completely opposite to the present results. Therefore, it is necessary to consider not only minimizing the friction coefficient but also maximizing the load capacity in the future.

REFERENCES

[1] D. B. Hamilton, J. A. Walowit, C. M. Allen. A Theory of Lubrication by Microirregularities, *J. Basic Eng*. (1966), 88: 177-185

[2] I. Etsion, L. Burstein, A Model for Mechanical Seals with Regular Microsurface Structure. *Tribology Transactions*, Vol. 39, (1996)

[3] H.L. Costa, I.M. Hutching, Hydrodynamic lubrication of textured steel surfaces under reciprocating sliding conditions, *Tribology International*, Vol. 40, (2007) 8:1227-1238.

[4] Cong Shen, M.M. Khonsari, Numerical optimization of texture shape for parallel surfaces under unidirectional and bidirectional sliding, Tribology International, Vol.82, (2015), 1-11.

[5] S. Sasaok, T. Kurahashi, Proposal of texture shape optimization algorithm under constant load condition and considerations on new shape update equation (Texture shape optimization for minimization of friction coefficient), Journal of Fluid Science and Technology, Vol. 15, 3:1-20, (2020).

[6] H. Kodama, S. Nakamae, M. Harada, D. Wada, K. Ohashi, Abrasive jet machining for the microprofile control patterning of herringbone grooves, *Precision Engineering*, Vol.72, (2021), 527-542.

[7] Z. Shena,F. Wang, Z. Chena, X. Ruan, H. Zeng, J. Wanga, Y. An, X. Fan, Numerical simulation of lubrication performance on chevron textured surface under hydrodynamic lubrication, Tribology International, Vol.154, (2021).

[8] T. Zhirong, M. Xiangkai, M. Yi, P. Xudong, Shape optimization of hydrodynamic textured surfaces for enhancing load-carrying capacity based on level set method, Tribology International, Vol.162, (2021)